# XKD: Cross-modal Knowledge Distillation with Domain Alignment for Video Representation Learning

Pritam Sarkar <sup>1,2</sup> Ali Etemad <sup>1</sup> Queen's University, Canada <sup>2</sup>Vector Institute

{pritam.sarkar, ali.etemad}@queensu.ca
https://pritamqu.github.io/XKD

# **Abstract**

We present XKD, a novel self-supervised framework to learn meaningful representations from unlabelled video clips. XKD is trained with two pseudo tasks. First, masked data reconstruction is performed to learn modality-specific representations. Next, self-supervised cross-modal knowledge distillation is performed between the two modalities through teacher-student setups to learn complementary information. To identify the most effective information to transfer and also to tackle the domain gap between audio and visual modalities which could hinder knowledge transfer, we introduce a domain alignment strategy for effective cross-modal distillation. Lastly, to develop a general-purpose solution capable of handling both audio and visual streams, a modalityagnostic variant of our proposed framework is introduced, which uses the same backbone for both audio and visual modalities. Our proposed cross-modal knowledge distillation improves linear evaluation top-1 accuracy of video action classification by 8.4% on UCF101, 8.1% on HMDB51, 13.8% on Kinetics-Sound, and 14.2% on Kinetics400. Additionally, our modality-agnostic variant shows promising results in developing a general-purpose network capable of handling different data streams. The code is released on the project website.

# 1. Introduction

Self-supervised learning aims to learn meaningful representations from unlabelled data with no human supervision [14, 15, 28, 38]. Using self-supervision, recent multimodal methods [5, 35, 37, 39, 40, 48] have shown great promise in learning effective representations from videos. In general, multimodal frameworks leverage the existing information in both data streams to learn better representations for downstream tasks toward either modality (or both). Recent audio-visual frameworks aim to perform *information sharing* between networks to further enrich the learned rep-

resentations [1,4,9,16,47]. However, effective cross-modal knowledge sharing between audio and video is particularly challenging due to the inherent diversity, complexity, and domain-specific nature of each modality, as well as the existence of substantial domain gaps between them [16,47].

In this work, we aim to perform effective information sharing between audio and video streams to obtain more generalized representations for downstream tasks. To this end, we propose a novel self-supervised framework called XKD, which stands for Cross-modal Knowledge Distillation. Our approach consists of two sets of pseudo-tasks, (i) masked data modelling and (ii) cross-modal knowledge distillation. The former is performed to learn modality-specific information, while the latter distills and transfers knowledge across modalities to further improve the learned representations. To allow for stable and effective information exchange between modalities, our method first performs feature refinement to identify 'what to transfer' based on cross-modal feature relevance, followed by minimizing the domain discrepancy to align the two representations. Additionally, we introduce a modality-agnostic (MA) variant of our method to tackle the challenging task of learning from both modalities using a unified network (shared backbone). Modality-agnostic methods are particularly useful given their ability to accept different data streams and solve a variety of tasks using the same network. Moreover, they ease the challenge of designing individual models for each modality, thus attracting attention in recent studies [2,25].

Inspired by the recent success of Transformers in different domains [20, 22, 26, 29], we use ViT [21] as the backbone of our framework for both audio and visual modalities. We use the popular Kinetics400 [31] to pretrain the framework. The pretrained backbones are then evaluated on multiple datasets on a variety of downstream tasks. More specifically, UCF101 [50], HMDB51 [33], Kinetics-Sound [6], and Kinetics400 [31] are used for action classification. Additionally, ESC50 [44] and FSD50K [24] are used for sound classification.

<sup>&</sup>lt;sup>1</sup>We use 'data' as a generic term for both audio and visual streams.

Our contributions are summarized as follows:

- We introduce a novel self-supervised framework for video representation learning through cross-modal knowledge distillation. Our model tackles two important challenges, namely feature transferability and domain alignment, which enable knowledge to be effectively shared between the two modalities. To the best of our knowledge, XKD is the first self-supervised cross-modal knowledge distillation framework for learning audio and visual modalities.
- Rigorous experiments show that our approach achieves strong results on a variety of downstream benchmarks including UCF101, HMDB51, Kinetics-Sound, FSD50K, ESC50, and Kinetics400. These experiments show the efficacy of XKD in improving video action classification accuracy by 8.1% to 14.2%. Furthermore, we perform indepth ablation studies and validate different components of our proposed framework.
- To create a general-purpose architecture capable of tackling diverse types of modalities, we also train XKD in a modality-agnostic fashion, where the same backbone is used for both audio and visual streams. While as expected, a slight performance drop is observed (e.g., 3.2% on both HMDB51 and UCF101), in comparison to the modality-specific variant, the overall performance shows considerable promise.

# 2. Related Work

Video-based Self-supervised Learning. Self-supervised learning has been widely used in a variety of different areas, including the challenging task of video representation learning [49]. Several prior works have attempted to learn video representations through both uni-modal [23, 30, 44] as well as multi-modal [3, 40, 45] pretraining. For example, prior works have explored self-supervised frameworks for learning video representations through contrastive [3, 39, 40], noncontrastive [45, 48], and deep clustering [5, 8] techniques.

Masked Data Modelling. Inspired by the success of BERT [20] in natural language processing, several prior works have attempted to learn meaningful representations through reconstruction of masked (corrupted) inputs. Such method employs encoder-decoder setups, where the encoder compresses the inputs into a lower dimension, while the decoder is trained for reconstruction. This simple approach shows great promise in different domains including image [10, 12, 29], video [22, 53, 54], and audio [17, 26, 42] among others.

Cross-modal Knowledge Distillation. The main goal of cross-modal knowledge distillation is to transfer knowledge across different modalities [1, 4, 9, 16, 19, 47]. For example, [1, 47] attempted knowledge distillation between audio teachers and video students to improve visual representations. Cross-modal knowledge distillation amongst different visual modalities has been performed in [19], where a pretrained optical flow teacher is used to improve RGB student's

representation. Distinct from prior works where the teacher is already been pretrained in a supervised manner, we aim to perform cross-modal knowledge distillation using teachers with no prior knowledge. In particular, we train both the teachers and students in an online fashion from scratch without using any class labels.

Modality-agnostic Networks. While modality-specific models have been the preferred approach toward developing representation learning solutions due to their strong performance, they do not have the ability to learn from multiple modalities using the same backbone, which makes them harder to develop. Recently, [2, 25] introduced modality-agnostic models capable of learning different modalities using the same backbones. In our paper, we attempt to develop modality-agnostic variants of our solution which can handle 2 very different modalities, i.e., audio and video.

# 3. Method

# 3.1. Overview

Figure 1 presents an overview of our framework. Our method consists of two sets of auto-encoders for audio  $(\theta^a_{ae})$  and video  $(\theta^v_{ae})$ . First, we train these auto-encoders to reconstruct the masked inputs, which helps the encoders  $(\theta^a_e$  and  $\theta^v_e)$  to learn modality-specific information. Next, to transfer knowledge between modalities in order to learn stronger representations, we align the two domains by identifying the most transferable features and minimizing the domain gaps. Finally, audio  $(\theta^a_t)$  and video  $(\theta^v_t)$  teachers are employed to provide cross-modal supervision to the opposite modalities. The details of our proposed method are mentioned below.

# 3.2. Data Embedding

Let be given video clip x, where the visual frames and audio spectrograms are denoted as  $x_v$  and  $x_a$ , respectively. We create 'global' and 'local' views from each modality which are then used by the teachers and students respectively. First, we apply augmentations on  $x_v$  and  $x_a$  to generate the global views as  $x_v^g$  and  $x_a^g$ . Next, we generate n local views  $x_v^l$  and  $x_a^l$  from  $x_v$  and  $x_a$  respectively, where  $x_v^l$  $\{x^l_{v1},\dots,x^l_{vn}\}$  and  $x^l_a=\{x^l_{a1},\dots,x^l_{an}\}.$  Specifically,  $x^l_{ai}$ is an augmented time-frequency crop of  $x_a$  and  $x_{vi}^l$  is an augmented spatio-temporal crop of  $x_v$ . To further elaborate,  $x_v^l$  and  $x_a^l$  are differently augmented than  $x_v^g$  and  $x_a^g$ . First, both local and global views of audio and visual inputs are projected into an embedding space. For example,  $x_a \in$  $\mathbb{R}^{F \times T_a}$  are reshaped into  $N_a$  smaller patches of size  $f \times t_a$ , where  $N_a = F/f \times T_a/t_a$ . Next, we reshape the videos  $x_v \in \mathbb{R}^{T_v \times H \times W \times C}$  into  $N_v$  smaller cuboids of size  $t_v \times W \times C$  $h \times w \times C$ , where  $N_v = T_v/t_v \times H/h \times W/w \times C$ . Finally, the spectrogram patches and visual cuboids are flattened into vectors and linearly projected onto the embedding space, which are then fed to the encoder backbones.

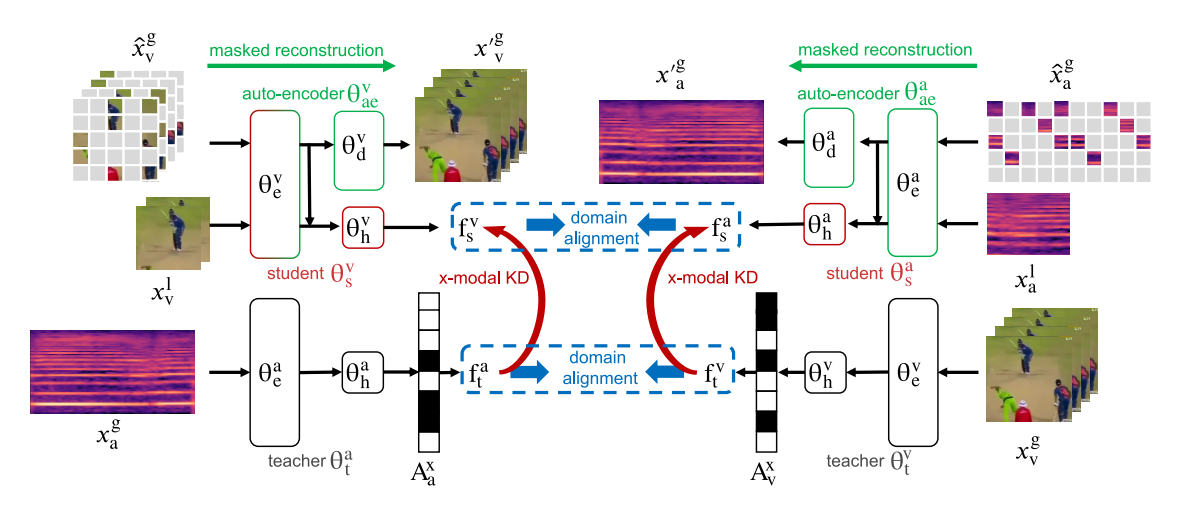


Figure 1. An overview of our proposed framework is presented. Here, auto-encoders ( $\theta_{ae}$ , which consist of  $\theta_e$  and  $\theta_d$ ) are used for masked reconstruction. To successfully perform cross-modal knowledge distillation, the two domains are first aligned. Next, the student networks ( $\theta_s$ , which consist of  $\theta_e$  and  $\theta_h$ ) are used to further distill knowledge from their respective cross-modal teachers ( $\theta_t$ ).

# 3.3. Masked Data Modelling

Inspired by the recent success of pretraining with masked reconstruction in different domains [11, 12, 20, 26, 29, 42, 53, 54], we first perform masked data modelling to learn modality-specific representations. The masked reconstruction employs an autoencoder  $\theta_{ae}$ , which itself consists of an encoder  $\theta_e$  and a decoder  $\theta_d$ . Let x be the input, which can be further expressed as a sequence of tokens  $\{x_i\}_{i=1}^N$ , as described in Section 3.2. Here, we randomly mask some of the input tokens with  $m \in \{0,1\}^N$ , hence the masked tokens  $x^{[m]}$  are represented as  $\{x_i|m_i=1\}_{i=1}^N$  while the corrupted inputs  $\hat{x}$  are represented as  $\{x_i|m_i=0\}_{i=1}^N$ . Further, we drop the masked tokens  $x^{[m]}$  before feeding the input to  $\theta_{ae}$  for computational efficiency [2, 29]. We train  $\theta_{ae}$  to reconstruct x based on input  $\hat{x}$ . Here,  $\theta_{ae}$  is trained to minimize the reconstruction loss  $\mathcal{L}_{recon}$ , expressed as:

$$\mathcal{L}_{recon}(\theta_{ae}(\hat{x}), x^{[m]}) = \frac{1}{N_m} \sum_{i=1}^{N_m} (\theta_{ae}(\hat{x}_i) - x_i^{[m]})^2.$$
 (1)

In particular, using Eq. 1, we define the video and audio reconstruction losses as  $\mathcal{L}^v_{recon}$  and  $\mathcal{L}^a_{recon}$  for given inputs  $x^g_v$  and  $x^g_a$ , to train  $\theta^v_{ae}$  and  $\theta^a_{ae}$ , respectively. Here  $\theta^v_{ae}$  and  $\theta^a_{ae}$  denote video and audio auto-encoders. To jointly train the audio-visual masked autoencoder, we define the final reconstruction loss  $\mathcal{L}_{ae}$  as:

$$\mathcal{L}_{ae} = \mathcal{L}_{recon}(\theta_{ae}^{v}(\hat{x}_{v}^{g}), x_{v}^{g[m]}) + \mathcal{L}_{recon}(\theta_{ae}^{a}(\hat{x}_{a}^{g}), x_{a}^{g[m]}) \quad (2)$$

# 3.4. Knowledge Distillation with Domain Alignment

To facilitate cross-modal knowledge sharing we adopt a teacher-student setup [52]. The teacher  $(\theta_t)$  and student  $(\theta_s)$  are comprised of a backbone and a projector head  $(\theta_h)$ , where the teacher and student network architectures are the

same but differently parameterized. Moreover, we parameterize  $\theta_s$  as  $\{\theta_e, \theta_h\}$ , where  $\theta_e$  is the same encoder used in reconstruction (explained in the previous subsection) and  $\theta_h$  is a newly added projector head. We define  $\theta_s^v$  and  $\theta_s^a$  as video and audio students, whereas,  $\theta_t^v$  and  $\theta_t^a$  are denoted as video and audio teachers.

As mentioned earlier, cross-modal knowledge distillation between audio and video is particularly difficult due to the inherent diversity, complexity, and domain-specific nature of these two modalities. To tackle this, we perform domain alignment to identify the most transferable features and minimize the domain discrepancy. The proposed domain alignment ensures meaningful target distributions are set by the teachers in order to perform successful cross-modal knowledge distillation.

**Domain Alignment.** Both the audio and video carry rich and diverse set of information about the source. Therefore, first, we identify the most transferable features by re-weighting the teachers' representations based on their cross-modal feature importance through a soft-selection process. Specifically, we obtain the cross-modal attention maps to calculate the cross-modal feature importance with respect to the corresponding modalities. In order to calculate the cross-modal attention maps, we first extract the modality-specific attention maps (*A*) from the last attention layers of the teacher networks as:

$$A = \operatorname{softmax}(Q^{\text{[CLS]}} \circ \frac{K^T}{\sqrt{d}}). \tag{3}$$

Here, Q denotes the query, K is the key, and V is the value. Specifically,  $A \in \mathbb{R}^{H \times N}$  is calculated as the correlation between the query (Q) embedding of the class token CLS and the key (K) embeddings of all the other patches or cuboids. Note, H denotes the number of attention heads

and N denotes the number of patches or cuboids. We obtain the visual attention  $A_v \in \mathbb{R}^{H \times N_v}$  and audio attention  $A_a \in \mathbb{R}^{H \times N_a}$  as per Eq. 3. Next, we obtain the respective cross-modal attention maps as  $A_v^{\times}$  and  $A_a^{\times}$  as:

$$A_{v}^{\times} = \left(\frac{1}{N_{a}} \sum_{i=1}^{N_{a}} A_{v} \circ A_{a}^{T}\right) / \left(\frac{1}{N_{v}} \sum_{i=1}^{N_{v}} A_{v}\right);$$

$$A_{a}^{\times} = \left(\frac{1}{N_{v}} \sum_{i=1}^{N_{v}} A_{v} \circ A_{a}^{T}\right) / \left(\frac{1}{N_{a}} \sum_{i=1}^{N_{a}} A_{a}\right).$$
(4)

Here,  $\frac{1}{N_v}\sum_{i=1}^{N_v}A_v$  and  $\frac{1}{N_a}\sum_{i=1}^{N_a}A_a$  are used as a scaling factor to re-scale the computed attention maps in their previous range for numerical stability. Accordingly, we obtain  $A_v \circ A_a^T \in \mathbb{R}^{H \times N_v \times N_a}$  and  $A_a \circ A_v^T \in \mathbb{R}^{H \times N_a \times N_v}$ . We identify the most transferable features obtained from the teachers as  $f_t^v$  and  $f_t^a$ , through  $refine(\theta_t^v(x_v^g), A_v^\times)$  and  $refine(\theta_t^a(x_a^g), A_a^\times)$  respectively. Here  $A_v^\times$  and  $A_a^\times$  are used to re-weight the visual and audio representations respectively. We formulate refine as:

$$refine(\theta_t(x^g), A^{\times}) = \theta_t(x^g) \circ \frac{1}{H} \sum_{h=1}^H A_h^{\times} \circ \Omega,$$
 (5)

where  $\Omega$  is a non-negative scalar defined as the ratio of prior and posterior energy, expressed as:

$$\Omega = \frac{\|\theta_t(x^g)\|_2^2}{\|\theta_t(x^g) \circ A^{\times}\|_2^2}.$$
 (6)

Next, to improve the knowledge transferability, we reduce the domain gaps by minimizing the Maximum Mean Discrepancy (MMD) [27] loss, estimated as:

$$\mathcal{L}_{mmd}(\mathbb{P}_a, \mathbb{P}_v) = \| \mathbb{E}_{x_a \sim \mathbb{P}_a}[k(\cdot, x_a)] - \mathbb{E}_{x_v \sim \mathbb{P}_v}[k(\cdot, x_v)] \|_{\mathcal{H}_k}.$$

Here  $x_a$  and  $x_v$  are drawn from distributions  $\mathbb{P}_a$  and  $\mathbb{P}_v$  respectively. Additionally,  $\|\cdot\|_{\mathcal{H}_k}$  is the RKHS norm [27] and and k represents the Gaussian kernel with bandwidth  $\sigma$ , written as:

$$k(x_a, x_v) = \exp\left(\frac{-\parallel x_a - x_v \parallel^2}{2\sigma^2}\right). \tag{8}$$

Using Eq. 7, we define domain alignment loss  $\mathcal{L}_{da}$  as:

$$\mathcal{L}_{da} = \mathcal{L}_{mmd}(f_s^v, f_s^a) + \mathcal{L}_{mmd}(f_t^v, f_t^a). \tag{9}$$

Here,  $f_s^a$  and  $f_s^v$  refer to audio and visual representations obtained from  $\theta_s^a$  and  $\theta_s^v$  respectively.

**Knowledge Distillation.** We perform knowledge distillation between modalities to provide cross-modal supervision in order to learn more generalized representations. We train the student networks to match the distribution of the cross-modal teacher networks. Specifically, we train  $\theta_s^v$  to match the distribution of  $\theta_t^a$ , while  $\theta_s^a$  is trained to match the distribution

of  $\theta^v_t$ . It has previously shown in [13] that normalizing the teacher's output is a key step when performing knowledge distillation. Accordingly, we normalize  $f^a_t$  and  $f^v_t$  with a 'mean' calculated based on the current batch statistics, which helps the teachers' outputs be more uniformly distributed. Additionally, to prevent abrupt updates of batch means, we slowly update the 'means' using an exponential moving average (EMA). Finally, we minimize the cross-entropy loss H(a,b) formulated as  $-a\log b$ , where a and b represent the output probability distributions of  $\theta_t$  and  $\theta_s$  respectively. Here, the probability P over J distributions is obtained by using a softmax function with the temperature parameter  $\tau$ , where  $0 < \tau < 1$  used to sharpen the distribution as:

$$P(f^{(i)}) = \frac{\exp(f^{(i)}/\tau)}{\sum_{i=1}^{J} \exp(f^{(j)}/\tau)}.$$
 (10)

Accordingly, we define the cross-modal knowledge distillation loss  $\mathcal{L}_{kd}$  as:

$$\mathcal{L}_{kd} = -P(f_t^v) \log(P(f_s^a)) - P(f_t^a) \log(P(f_s^v)). \tag{11}$$

#### 3.5. Final Loss

To train XKD, we define the final loss function as the combination of reconstruction, domain alignment, and cross-modal knowledge distillation losses expressed as:

$$\mathcal{L}_{xkd} = \lambda_{ae} \times \mathcal{L}_{ae} + \lambda_{da} \times \mathcal{L}_{da} + \lambda_{kd} \times \mathcal{L}_{kd}. \tag{12}$$

Here,  $\lambda_{ae}$ ,  $\lambda_{da}$ , and  $\lambda_{kd}$  are the loss coefficients corresponding to the three terms, respectively. Empirically, we set  $\lambda_{ae}$ ,  $\lambda_{da}$ , and  $\lambda_{kd}$  as 5, 1, and 1 respectively. It should be noted that  $\mathcal{L}_{xkd}$  is only used to train  $\theta_s$  and  $\theta_{ae}$ , not  $\theta_t$ . Following [11, 13, 52], EMA is used to update  $\theta_t^a$  and  $\theta_t^v$  as:

$$\theta_t^a \leftarrow \lambda_a \theta_t^a + (1 - \lambda_a) \theta_s^a \text{ and } \theta_t^v \leftarrow \lambda_v \theta_t^v + (1 - \lambda_v) \theta_s^v,$$
(13)

where  $\lambda_a$  and  $\lambda_v$  are the EMA coefficients corresponding to  $\theta^a_t$  and  $\theta^v_t$ . We present the proposed method in Algorithm 1.

# 3.6. Modality Agnostic Variant

We take our proposed approach a step forward and attempt to train it in a modality-agnostic fashion with the goal of developing a 'general' network capable of handling both modalities. This is a very challenging task in the context of our work given the very diverse nature of audio and video streams. We briefly explore three different modality-agnostic setups, (a) modality-agnostic teacher and modality-agnostic student (XKD-MATS), (b) modality-agnostic teacher with modality-specific student (XKD-MAT), and (c) modality-agnostic student with modality-specific teacher (XKD-MAS). As the name suggests, in XKD-MATS the audio and visual teachers share their backbones, and so do the audio and visual students. In the case of XKD-MAT, the

# Algorithm 1 XKD Training Algorithm.

```
1: Input: x_v, x_a
 2: Initalize: \theta_d^v, \theta_d^a, \theta_s^v, \theta_s^a, \theta_t^v, \theta_t^a
 3: for t in iterations do
               Obtain x_v^g and x_v^l from x_v
 4:
               Obtain x_a^g and x_a^l from x_a
 5:
               Reconstruction:
               f_{sv}^g = \theta_e^v(\hat{x}_v^g); f_{sa}^g = \theta_e^a(\hat{x}_a^g)
  6:
               \mathcal{L}_{ae} \!=\! \mathcal{L}_{recon}(\theta_d^v(f_{sv}^g), x_v^{g[m]}) \!+\! \mathcal{L}_{recon}(\theta_d^a(f_{sa}^g), x_a^{g[m]})
  7:
               Cross-modal knowledge distil. w/ domain alignment:
               with no-gradient:
 8:
                      f_{tv}^g = \theta_t^v(x_v^g); f_{ta}^g = \theta_t^a(x_a^g)
  9:
                     \begin{array}{l} \text{Obtain } A_v^{\times}, A_a^{\times} \\ f_t^v = refine(f_{tv}^g, A_v^{\times}) \\ f_t^a = refine(f_{ta}^g, A_a^{\times}) \end{array}
                                                                                                                 ⊳ Eq. 4
10:
                                                                                                                 ⊳ Eq. 5
11:
12:
                                                                                                                 ⊳ Eq. 5
               f_{sv}^{l} = \theta_{s}^{v}(x_{v}^{l}); f_{sa}^{l} = \theta_{s}^{a}(x_{a}^{l})
13:
               f_s^v = \text{Concat}\left(\theta_h^v(f_{sv}^g), f_{sv}^l\right)
14:
               f_s^a = \text{Concat}\left(\theta_h^a(f_{sa}^g), f_{sa}^l\right)
15:
               \mathcal{L}_{da} = \mathcal{L}_{mmd}(f_s^v, f_s^a) + \mathcal{L}_{mmd}(f_t^v, f_t^a)
16:
               \mathcal{L}_{kd} = -P(f_t^v)\log(P(f_s^a)) - P(f_t^a)\log(P(f_s^v))
17:
               \mathcal{L}_{xkd} = \lambda_{ae} \times \mathcal{L}_{ae} + \lambda_{da} \times \mathcal{L}_{da} + \lambda_{kd} \times \mathcal{L}_{kd}
18:
               Update \theta_d^v, \theta_d^a, \theta_s^v, \theta_s^a based on \mathcal{L}_{xkd}
19:
               Update \theta_t^v and \theta_t^a
20:
                                                                                                               ⊳ Eq. 13
21: end for
22: Output: \theta_s^v, \theta_s^a, \theta_t^v, \theta_t^a
```

backbones of audio and visual teachers are shared, but the students use modality-specific backbones. Lastly, in XKD-MAS, the audio and visual students share their backbones, while the audio and visual teachers use modality-specific backbones. Please note that in all the setups, we use the Eq. 13 to update the teacher using their respective students. Moreover, given the need to reconstruct different modalities, all of the variants use modality-specific decoders and input projection layers. The rest of the setups remain the same as the original XKD. All three variants are trained with  $\mathcal{L}_{xkd}$  (see Eq. 12). We present our findings in Section 4 and further details of the variants are presented in the Appendix C.

# 4. Experiments and Results

# 4.1. Implementation Details

We use a total of 6 datasets in this study, namely Kinetics400 [31], Kinetics-Sound [6], UCF101 [50], HMDB51 [33], ESC50 [43], and FSD50K [24]. The details for all these datasets are provided in Appendix B. The large-scale Kinetics400 is used to pretrain our proposed XKD and the other datasets are used for downstream evaluation. We choose ViT-Base (ViT-B) [21] as the backbone of our framework for both audio and video modalities, due to its stability in performance across different data streams [7, 26, 29]. The details of the architecture are presented in Appendix C. To train the network, we downsample the video input at 8 FPS and resize the frame resolution at  $112^2$ . Additionally, we re-sample the

audio waveforms at 16 kHz. and generate mel-spectrograms using 80 mel filters, where we set the hop size at 14.3 milliseconds (ms) and FFT window length at 1024. Next, we create global and local views for both audio and video. We use 4 seconds of audio-visual input for the global views. Followed by the local views are generated by taking random temporal segments of 1 second unless stated otherwise. The final input sizes to the teachers are  $3\times32\times112^2$  and  $80\times448$ . Similarly, the input sizes to the students are  $3 \times 8 \times 96^2$  and  $80 \times 112$ , for video and audio respectively. Moreover, the inputs to the encoders for masked reconstructions are the same as the input to the teacher networks, except they are heavily masked. We use a patch size of  $4 \times 16$  for audio spectrogram and cuboid size of  $4 \times 16^2$  for video input. It should be noted that, to the best of our knowledge, this is the first time such low frame resolutions are used with ViT [21] while keeping the spatial patch as 16<sup>2</sup>. To further clarify, we use frame resolution of 112<sup>2</sup> and 96<sup>2</sup>, whereas, spatial resolutions of  $224^2$  and  $384^2$  are mostly used during pretraining amongst the earlier works [2, 13, 22, 29, 53]. Our setup saves the computation requirement by at least  $4\times$  which makes it possible to train XKD with limited computation resources.

Please note, during ablation and design exploration, we pretrain the models for 400 epochs and perform linear evaluations using the split-1 of UCF101, HMDB51, and ESC50, unless stated otherwise. We present the additional experiment setup details in Appendix C.

#### 4.2. Ablation Studies

Following, we present the findings of our thorough ablation studies. When ablating our proposed framework we encounter a few setups in which our model fails to perform cross-modal knowledge distillation due to collapse and/or instability. To identify a potential collapse, we monitor the Kullback–Leibler divergence (KLD) loss between the cross-modal teachers and students (i.e., between audio-teacher and video-student and vice versa), as it becomes zero when the outputs become a constant vector. Please note that we do not optimize the KLD loss for training our framework, and simply visualize it to track pretraining stability.

# 4.2.1 Effect of cross-modal knowledge distillation

As discussed, the proposed XKD is pretrained to solve two pseudo tasks, masked data modelling and cross-modal knowledge distillation. Therefore, to obtain an accurate understanding of the effect of cross-modal knowledge distillation, we separately perform masked data reconstruction on video  $(\mathcal{L}^v_{recon})$  and audio  $(\mathcal{L}^a_{recon})$  modalities. We also jointly train the audio-video masked auto-encoder  $(\mathcal{L}_{ae})$  and compare it to XKD . We pretrain all these variants for the full training schedule of 800 epochs, followed by linear evaluation on the split-1 downstream benchmarks.

Loss		•	Audio			
1033	UCF101	HMDB51 (Acc@1)	KS	<b>K400</b> (Acc@1/5)	FSD50K (mAP@1)	ESC50 (Acc@1)
$\mathcal{L}_{recon}^{v}$	76.1	51.1	56.8	30.7/57.0	n/a	n/a
$\mathcal{L}^a_{recon}$	n/a	n/a	n/a	n/a	44.6	90.0
$\mathcal{L}_{ae}$	76.3	51.2	56.9	32.2/58.4	44.3	90.0
$\mathcal{L}_{xkd}$	<b>84.7</b> (↑ 8.4)	<b>59.3</b> († 8.1)	<b>70.7</b> († 13.8)	<b>46.4/71.6</b> († 14.2/13.2)	<b>45.8</b> († 1.5)	<b>91.0</b> († 1.0)

Table 1. Effect of cross-modal knowledge distillation. Note: the changes highlighted in green are calculated w.r.t.  $\mathcal{L}_{ae}$ , mAP: mean average precision, KS: Kinetics-Sound, K400: Kinetics400.

Visual representations. The results presented in Table 1 show that video representations significantly benefit from the cross-modal supervision obtained through knowledge distillation. In particular, cross-modal knowledge distillation improves video action recognition by 8.4%, 8.1%, and 13.8% on UCF101, HMDB51, and Kinetics-Sound, respectively. Furthermore, we challenge XKD on Kinetics400 in a linear evaluation setup which improves the top-1 accuracy by 14.2%. Interestingly, we do not notice any considerable improvements by jointly training the audio and visual masked auto-encoders ( $\mathcal{L}_{ae}$ ), specifically when evaluating on UCF101, HMDB51, and Kinetics-Sound. Additionally, we also train our framework with  $\mathcal{L}_{da}$  along with  $\mathcal{L}_{ae}$  (i.e., setting  $\lambda_{kd}$  as 0 in Eq. 12) and present the result in Appendix A, where we do not observe any significant benefits either.

Audio representations. In Table 1 we notice that the improvement in audio representations through cross-modal knowledge distillation is relatively less significant compared to visual representations. Specifically, XKD results in 1.5% and 1% improvement on FSD50K and ESC50 for sound classification. Our thorough literature review in this regard reveals that a similar phenomenon has also been noticed amongst earlier works [16, 47] that have attempted crossmodal knowledge distillation between audio and video in a semi-supervised setting (i.e., pretrained teachers are used to provide cross-modal supervision). We conclude that while audio-to-video knowledge distillation is highly effective, video-to-audio provides a less substantial improvement. To further study the reason behind this, we visualize the distributions of audio and video modalities using Kinetics 400. Interestingly, as shown in Figure 2, we observe that the distribution of audio is sharper than the video, which might be a better source for providing cross-modal supervision in a teacher-student setup.

# 4.2.2 Domain alignment

**Effect of**  $\mathcal{L}_{da}$ . First, we study the impact of our domain alignment step toward cross-modal knowledge distillation. To this end, we set the  $\lambda_{da}$  as zero in Eq. 12. We find that the KLD loss reaches zero after a few iterations. Additionally,

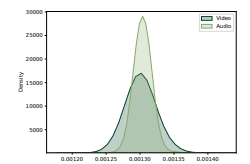


Figure 2. Distribution	Τ
of audio and visual rep-	V
resentations.	

	$\mathcal{L}_{ ext{da}}^{ ext{no.refine}}$	$\mathcal{L}_{\mathbf{da}}^{1}$	$\mathcal{L}_{\mathbf{da}}^{2}$	$\mathcal{L}_{\mathbf{da}}$ (default)
HMDB51	55.6	56.1	82.2	58.5
UCF101	79.3	81.1		82.6
ESC50	84.3	87.3		88.0

Table 2. Ablation study on  $\mathcal{L}_{\mathbf{da}}$  and it's variants.

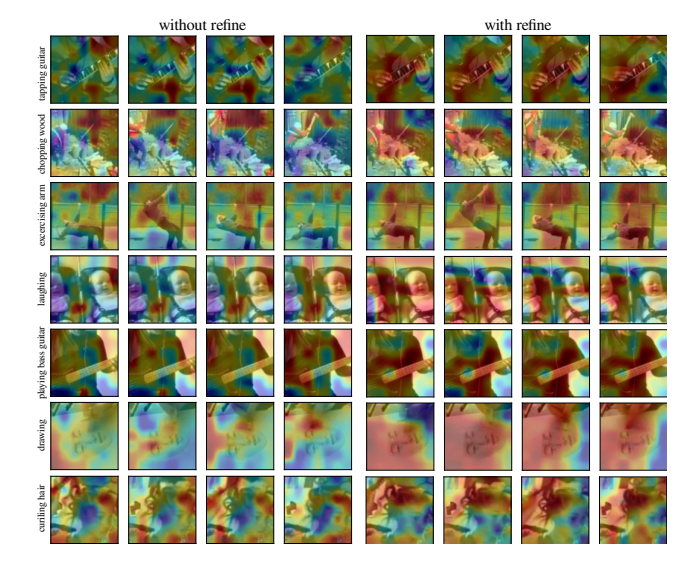


Figure 3. The effect of *refine* in identifying the most salient visual features (best viewed in color).

the  $\mathcal{L}_{kd}$  shows extreme oscillation and the model fails to perform cross-modal knowledge distillation, confirming the importance of minimizing domain discrepancies for effective cross-modal knowledge distillation. We present the training curves and additional discussions in Appendix A.

**Effect of** *refine*. Next, to study the impact of feature refinement in cross-modal knowledge distillation, we replace Eq. 9 with Eq. 14 in the final loss function Eq. 12.

$$\mathcal{L}_{da}^{no.refine} = \mathcal{L}_{mmd}(\theta_t^a(x_a^g), \theta_t^v(x_v^g)) + \mathcal{L}_{mmd}(f_s^v, f_s^a) \quad (14)$$

The results presented in Table 2 demonstrate that refine significantly improves downstream performance. Additionally, we visualize the features before and after refinement in Figure 3, which further confirms the ability of refine in identifying the most transferable and key features.

Variants of  $\mathcal{L}_{da}$ . Next, we explore a few variants of  $\mathcal{L}_{da}$  towards investigating the optimal setup for domain alignment. (i) First, we replace  $\mathcal{L}_{da}$  with  $\mathcal{L}_{da}^1$ , where instead of minimizing the MMD loss among teachers and among students, we aim to minimize the loss between the teachers and students, as  $\mathcal{L}_{da}^1 = \mathcal{L}_{mmd}(f_t^a, f_s^v) + \mathcal{L}_{mmd}(f_t^v, f_s^a)$ . (ii) Next, we study the effect of optimizing  $\mathcal{L}_{da}^1$  in addition to  $\mathcal{L}_{da}$ , expressed as:  $\mathcal{L}_{da}^2 = \mathcal{L}_{da} + \mathcal{L}_{da}^1$ . (iii) Finally, we

	XKD-	MATS	XK	D-MAS	XKD		
	Teacher (ma)	Student (ma)	Teacher	Student (ma)	Teacher	Student	
HMDB51	53.5	52.4	56.4	55.2(\ 3.2)	58.4	57.8	
UCF101	80.3	80.0	81.9	$81.5(\downarrow 3.2)$	84.7	84.4	
ESC50	$90.3(\downarrow 0.7)$	89.8	91.0	89.5	91.0	90.3	

Table 3. We present a performance comparison between modality-agnostic vs. modality-specific variants, and teachers vs. students. We highlight the performance drop in the best modality-agnostic variants w.r.t. the modality-specific model. ma: modality-agnostic.

Method	Dataset	M	Backbone	Input	Patch	# Tokens	U101	H51
VideoMAE [53]	K400	V	ViT-B	$16 \times 224^{2}$			80.0	54.3
VideoMAE <sup>1</sup> [53]	K400	V	ViT-B	$16\times112^2$	$2 \times 16^2$	392	77.1	51.6
VideoMAE <sup>2</sup>	K400	V	ViT-B	$32 \times 112^{2}$	$4 \times 16^2$	392	78.9	51.5
XKD	K400	VA	ViT-B	$32 \times 112^{2}$		392	83.8	57.4
XKD-MATS	K400	VA	ViT-B	$32 \times 112^2$		392	80.1	53.1
XKD-MAS	K400	VA	ViT-B	$32 \times 112^{2}$	$4 \times 16^2$	392	81.7	55.1
BraVe [45]	AS	VA	TSM-50	$32\!\times224^2$	-	-	93.0	69.4
VATT [2]	AS+HT	VAT	ViT-M	$32\!\times 224^2$	$4\times 16^2$	1568	89.6	65.2
VATT-MA [2]	AS+HT	VAT	ViT-M	$32\!\times224^2$	$4 \times 16^2$	1568	84.4	63.1

<sup>&</sup>lt;sup>1</sup> Trained using the official codes/weights released. <sup>2</sup> Our implementation.

Table 4. SOTA comparison on video action recognition using linear evaluation. Note: Dataset, M, Input, Patch, and # Tokens refer to the pretraining setup. Please see the abbreviations. <sup>2</sup>

Method	Dataset	M	Backbone	Input	Patch	# Tokens	Top1	Top5
BEVT [54] VideoMAE [53] VideoMAE [53] XKD	K400 K400	V V VA	ViT-B ViT-B ViT-B	$32 \times 224^{2}$ $16 \times 224^{2}$ $16 \times 112^{2}$ $32 \times 112^{2}$ $32 \times 112^{2}$	$2 \times 16^{2}$ $2 \times 16^{2}$ $4 \times 16^{2}$	392	65.2 <b>77.6</b>	n/a 94.7 85.7 <b>92.9</b>
XKD-MATS XKD-MAS	K400 K400	VA VA		$32 \times 112^2$ $32 \times 112^2$				92.2 92.1
VATT [2] VATT [2] VATT-MA [2]	AS+HT AS+HT AS+HT	VAT	ViT-M	$32 \times 224^{2}$ $32 \times 224^{2}$ $32 \times 224^{2}$	$4 \times 16^2$	1568 1568 1568		94.9 95.6 94.9

Table 5. SOTA comparison on video action recognition using finetuning on Kinetics400. Note: Dataset, M, Input, Patch, and # Tokens refer to the pretraining setup. Please see the abbreviations.<sup>2</sup>

study the effect of minimizing MMD loss only between the teachers as:  $\mathcal{L}^3_{da} = \mathcal{L}_{mmd}(f^a_t, f^v_t)$ . The results presented in Table 2 indicate drops in performance when using  $\mathcal{L}^1_{da}$  and  $\mathcal{L}^2_{da}$ . Moreover, we observe that the cross-modal knowledge distillation fails when adopting  $\mathcal{L}^3_{da}$ . We present additional experiments on domain alignment in Appendix A.

# 4.3. Modality-agnostic Approach

We train the modality-agnostic variants for 800 epochs and perform linear evaluations using the split-1 of UCF101, HMDB51, and ESC50. The results presented in Table 3 are promising, as these variants show minor performance drops (e.g., 3.2% on both HMDB51 and UCF101, and 0.7% on ESC50) in comparison to the default XKD. Amongst modality-agnostic backbones, XKD-MATS works slightly better on ESC50, whereas, XKD-MAS shows better per-

Method	Dataset	M	E50	F50K
XDC [5]	K400	VA	78.0	-
AVID [40]	K400	VA	79.1	-
CrissCross [48]	K400	VA	86.8	-
XKD	K400	VA	89.4	45.8
XKD-MATS	K400			43.4
XKD-MAS	K400	VA	87.3	43.0
BYOL-A [41]	AS	Α	-	44.8
MaskSpec [17]	AS	Α	89.6	-
MAE-AST [17]	AS	Α	90.0	-
VATT [2]	AS+HT	VAT	84.7	-
VATT-MA [2]	AS+HT	VAT	81.2	-

Table 6. SOTA comparison on sound
classification using linear evaluation.
Please see the abbreviations <sup>2</sup>

Method	A	V	A+V
CrissCross [48			
XKD			81.2
XKD-MATS	61.8	67.7	78.3
XKD-MAS	61.7	68.3	78.8

Table 7. SOTA comparison on multi-modal action classification using linear evaluation on Kinetics-Sound. Please see the abbreviations.<sup>2</sup>

	0.98	0.99	0.993	0.995	0.997	0.999
HMDB51 UCF101		0,.1	00.1	57.7 82.1	<b>58.5</b> 82.6	56.9 81.4
ESC50	86.5	85.6	86.7	84.8	88.0	84.4

Table 8. Effect of different EMA schedules.

formance on both UCF101 and HMDB51. However, XKD-MAT does not work due to an unstable teacher weight update schedule. As the teacher is shared but not the students, the weights of the teacher are updated by two students who are not necessarily synchronized. This leads to a degenerated solution (results not shown). We find that further research needs to be done to tackle such challenges, which is out-of-scope for this work and we plan to address in the future. Lastly, when comparing the performance between the teachers and students, teachers show slightly better performance on all the benchmarks and in all the setups.

#### 4.4. Comparing to the State-of-the-art

We notice large variability in the experiment setups among the prior works in terms of different network architectures [5,40,48] (i.e., ConvNet, Transformer), pretraining setups [2,22,26,32,53] (i.e., datasets, input resolutions, modalities), downstream evaluation protocols [2,53] (i.e., finetune, fc-tune, linear SVM), and others. In Tables 4, 5, 6, and 7 we provide our models' performance along with the experimental details necessary to consider, in comparison to the other leading methods. We present the details of the evaluation protocols in Appendix D.

Following [2,3,45], we report linear evaluation top-1 accuracy averaged over all the splits on UCF101 and HMDB51, and compare with the prior works. The results presented in Table 4 show that XKD outperforms VideoMAE [53] pre-

<sup>&</sup>lt;sup>2</sup>In Tables 4, 5, 6, and 7, M: Modalities, V: Video, A: Audio, T: Text, U101: UCF101, H51: HMDB51, E50: ESC50, F50K: FSD50K, AS: AudioSet (2M), HT: HowTo100M (100M), K400: Kinetics400 (240K).

			$0.04\!\to\!0.06 \\ 0.04\!\to\!0.06$				
HMDB51 UCF101		57.5 81.0	58.5	 	54.4	 	 52.7
ESC50	00.0	85.3	<b>82.6</b> 88.0		81.0 87.0		79.0 86.5

Table 9. Effect of different temperatu	tree in cross	-modal knowle	edge distillation

	Last	All
HMDB51 UCF101	55.1 79.7	
ESC50	83.5	88.0

Table 10. Effect of normalization layers in the projector head.

trained with  $224^2$  frame resolution by 3.8% and 3.1% on UCF101 and HMDB51. Moreover, XKD exceeds Video-MAE pretrained with  $112^2$  by 6.7% and 5.8% on UCF101 and HMDB51. Following [2,53,54], we finetune XKD on Kinetics400 and achieve a top-1 accuracy of 77.6%, outperforming VideoMAE [53] pretrained with  $112^2$  by 12.4%.

In Table 6, we compare the performance of our proposed method using linear evaluation on sound classification using two popular audio benchmarks ESC50 and FSD50K. Following [24,43], we report top-1 accuracy averaged over all the splits on ESC50 and mean average precision on FSD50K. XKD outperforms prior works [5,40,48] on ESC50 while pretrained on Kinetics400. Moreover, XKD and its modality-agnostic variants outperform VATT and VATT-MA [2] respectively, on ESC50 by 4.7% and 7.5%. It should be noted that VATT is pretrained with 136M videos, compared to ours which is only trained on 240K samples. Additionally, when evaluated on FSD50K, XKD outperforms BYOL-A [41] which is pretrained on the very large-scale AudioSet (2M).

Finally, we evaluate our proposed method in a multimodal setup using Kinetics-Sound. Following [48], we extract the audio and visual features and perform action classification using a linear SVM classifier utilizing the joint audio-visual embeddings. The results presented in Table 7 show that both XKD and its modality-agnostic variants outperform CrissCross in multi-modal action classification by 14.5% and 12.1%. Moreover, both XKD outperforms CrissCross on Kinetics-Sound when evaluated individually using audio and visual representations as well.

# 4.5. Analysis

lyze the key components of our proposed framework and redirect the reader to Appendix A for additional studies. **EMA.** We update the weights of the teachers using EMA as described in Eq. 13. In particular, we set the values of  $\lambda_a$  and  $\lambda_v$  using a cosine scheduler with a final value of 1. This means that we update the teachers more frequently at the beginning of training, and slow down their weight update towards the end of the training. This strategy results in a very smooth update of the networks' parameters and results in stable performance [52]. The results presented in Table 8 show that  $\lambda = 0.997$  works well on most of the benchmarks. **Temperature.** We study the effect of a wide range of tem-

Here we perform additional experiments to further ana-

perature settings ( $\tau$  in Eq. 10) in our proposed framework. The results presented in Table 9 show that a relatively lower temperature works well on the audio teacher (0.04 - 0.07), whereas a high temperature (0.1 - 0.11) is required for the video teacher. Please note that we keep the students' temperature fixed at 0.1. To find the best performance, we sweep a range of combinations and notice that for both audio and video teachers, increasing the temperatures from 0.04 to 0.06 works fairly well for both modalities. Additionally, we notice that setting fixed temperatures of 0.07 and 0.1 for audio and video teachers respectively, works slightly better on ESC50; however, a performance drop is noticed for video, specifically on HMDB51. We conjecture that carrying more information and thus the wider distribution of the video stream (see Figure 2) requires a higher temperature in order to further sharpen the distribution. Please note that unless mentioned otherwise, we use  $0.04 \rightarrow 0.06$  for both audio and video teachers throughout our experiments.

**Projector Head.** The configuration of the projector heads plays an important role in the performance of our method. We experiment with a variety of different setups including normalization, output dimension, and number of layers. Given the importance of the normalization strategy, we present the results for this experiment here, while the rest are provided in Appendix A. Here, in Table 10, we present the results for three setups, (a) no normalization, (b) normalization on the last layer, and (c) normalization on every layer. Our study shows that the cross-modal knowledge distillation fails in the absence of the normalization layer. We then observe that adding normalization on the last layer prevents the model from collapse, while adding normalization on every layer shows considerable improvements (see Table 10).

# 5. Summary

In this work, we propose XKD, a novel self-supervised framework to improve video representation learning using cross-modal knowledge distillation. To effectively transfer knowledge between audio and video modalities, XKD aligns the two domains by identifying the most transferable features and minimizing the domain gaps. Our study shows that cross-modal knowledge distillation significantly improves video representations on a variety of benchmarks. Additionally, to develop a general network with the ability to process different modalities, we introduce modality-agnostic variants

of our proposed method which show promising results in handling both audio and video using the same backbone.

# Acknowledgments

We are grateful to the Bank of Montreal and Mitacs for funding this research. We are thankful to SciNet HPC Consortium for helping with the computation resources.

# **Supplementary Material**

The organization of the supplementary material is as follows:

• Appendix A: Additional Experiments;

• Appendix B: Datasets;

• Appendix C: Pretraining Details;

• Appendix D: Downstream Evaluation;

# A. Additional Experiments

# A.1. Domain Alignment w/o Knowledge Distillation

Here we extend our earlier ablation study presented in Table 1 to further test the impact of domain alignment ( $\mathcal{L}_{da}$ ) in absence of cross-modal knowledge distillation. To this end we train our framework to minimize  $\mathcal{L}_{da}$  along with  $\mathcal{L}_{ae}$  (i.e., setting  $\lambda_{kd}$  to 0 in Eq. 12) for 800 epochs. The results presented in Table S1 show that without cross-modal knowledge distillation (w/o  $\mathcal{L}_{kd}$ ), the performance in video action classification on UCF101 and HMDB51 remains almost the same with respect to the masked reconstruction ( $\mathcal{L}_{ae}$ ). This shows that simply aligning the audio and video domains for masked reconstruction does not result in considerable benefit and that the improvements in XKD's performance are achieved due to the combination of cross-modal knowledge distillation and domain alignment.

#### A.2. Avoiding Collapse and Training Instability

Here we summarize the setups that cause a collapse and instability in cross-modal knowledge distillation. We identify three such instances, (i) without normalization layer in the projectors, (ii) without  $\mathcal{L}_{da}$ , and (iii) without normalizing the teacher's representations based on the current batch statistics (centering [13]). To identify collapse we mainly track the Kullback–Leibler divergence ( $\mathcal{L}_{kld}$ ) and Knowledge Distillation ( $\mathcal{L}_{kd}$ ) losses as shown in Figure S1. First, when no normalization layer is added in the projector head, the  $\mathcal{L}_{kld}$ loss becomes zero, which indicates that the models output a constant vector. Second, without  $\mathcal{L}_{da}$  the  $\mathcal{L}_{kld}$  loss also reaches zero (with minor spikes) which indicates training collapse. Lastly, we notice that without the centering, KLD does not become zero while the  $\mathcal{L}_{kd}$  reaches zero, which also indicates training collapse. Finally, to provide more insight into the training process, we present all the training curves of the default setup in Figure S2.

	$\mathcal{L}_{\mathbf{ae}}$	w/o $\mathcal{L}_{\mathrm{kd}}$	$\mathcal{L}_{\mathbf{xkd}}$
HMDB51	51.2	51.4	59.3
UCF101	76.3	77.8	84.7
ESC50	90.0	88.5	91.0

Table S1. Effect of domain alignment w/o knowledge distillation.

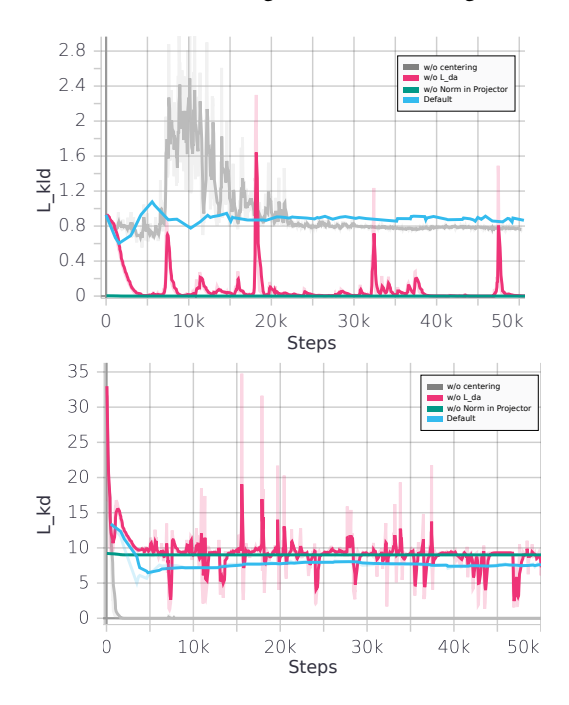


Figure S1. Visualizing pretraining instability and collapse in crossmodal knowledge distillation in the absence of centering, domainalignment, or normalization in the projector head.

# A.3. Feature Refinement

Here, we perform additional studies to evaluate our design choices for the refine step.

Cross-modal attention map. To perform feature selection, we use the cross-modal attention maps to refine the representations for effective knowledge distillation. We find that a potential alternative to our default Eq. 4 can be Eq. S1. In particular, the scaling operation in Eq. 4 can be simply replaced by a softmax function. We notice that this technique works slightly better on audio representations in comparison to our default setup; however, a considerable performance drop is noticed on visual representations. Please see the results in Table S2.

$$A_{v}^{'\times} = \operatorname{softmax}(\frac{1}{N_{p}} \sum_{i=1}^{N_{p}} A_{v} \circ A_{a}^{T});$$

$$A_{a}^{'\times} = \operatorname{softmax}(\frac{1}{N_{c}} \sum_{i=1}^{N_{c}} A_{v} \circ A_{a}^{T})$$
(S1)

**CLS token.** As mentioned in Eq. 3, by default we use the

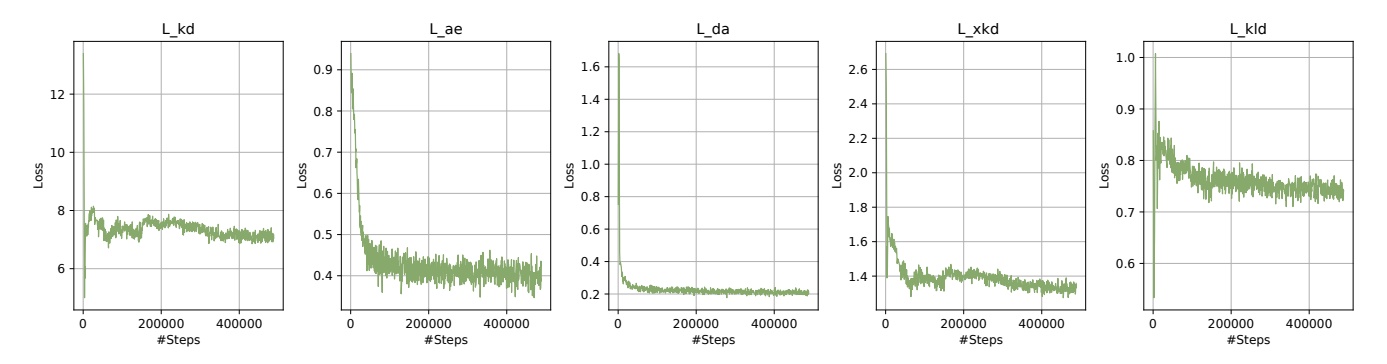


Figure S2. Stable training curves are presented.

	$\boldsymbol{A}'^{\times}$	w/o CLS	default
HMDB51	54.6	54.5	58.5
UCF101	79.8	79.3	82.6
ESC50	88.3	84.5	88.0

Table S2. Exploring different domain alignment setups.

Vis-Aud (sec.)	1 - 1	$2\!-\!2$	$2\!-\!1$	$1\!-\!2$	$4\!-\!1$
HMDB51	58.5	55.2	57.1	55.6	58.4
UCF101	82.6	81.1	82.3	81.0	82.6
ESC50	88.0	86.8	87.3	86.8	82.3

Table S3. Effect of different temporal window sizes for local views. Here **bold** shows the best and underline shows the worst results.

Vis-Aud (no.)	1 - 1	$1\!-\!2$	$2\!-\!1$	$2\!-\!2$	3 - 1
HMDB51	58.5	56.3	<b>58.8</b> 82.2 87.0	56.1	57.5
UCF101	82.6	79.5		79.0	<b>82.9</b>
ESC50	88.0	85.8		<b>90.8</b>	88.8

Table S4. Exploring the number of local views. We highlight the best results in **bold** and the worst with underline.

CLS tokens to obtain  $A_v$  and  $A_a$ , which are then used to generate  $A_v^{'\times}$  and  $A_a^{'\times}$ . Here, we explicitly study if CLS tokens are necessary in our framework. To test this, we modify Eq. 3 and calculate the intra-modal attention map as the correlation of the mean of the query embeddings and the key embeddings of all other patches. Please note that the rest of the setup remains the same. Table S2 shows that removing the CLS token significantly degrades the model performance on both audio and visual representations.

#### A.4. Local Views

We study the effect of the size of temporal windows used to create the local views for training the student networks. For the video stream, we create the local views by taking spatial crops of  $96 \times 96$  pixels and vary the temporal win-

	2	3	4
HMDB51	55.4	58.5	55.7
UCF101	81.0	82.6	81.0
ESC50	83.4	88.0	84.6

Table S5. Effect of different number of projector layers.

dows in the range of  $\{1, 2, 4\}$  seconds. Similarly for the audio stream, we explore temporal windows in the range of  $\{1, 2\}$  seconds. Our results presented in Table S3 reveal some interesting findings. First, local views comprised of audio and visual sequences of just 1 second work the best on all three benchmarks. Interestingly, we notice that the downstream audio classification performance drops significantly when XKD uses long visual local views (see column 4-1 in Table S3), while the downstream video classification performance remains more or less unchanged. On the other hand, we notice considerable performance drops on downstream video classification when using large audio segments to create the local views (see columns 2-2 and 1-2 in Table S3). These observations indicate that local views comprised of relatively shorter temporal windows are most effective when learning from the cross-modal teachers, which in turn results in improved downstream classification performance.

In addition to the length of the temporal window, we investigate the effect of varying the number of local views. This experiment shows that single local views for both audio and visual modalities work fairly well. We also find that adding more visual local views (e.g., 2 or 3) when using a single audio local view improves the performance on HMDB51 and UCF101, as shown in columns 2-1 and 3-1 in Table S4. Additionally, we notice that adding more audio local views worsens the model's performance in video classification (see columns 1-2 and 2-2 in Table S4). Lastly, we notice considerable improvements in sound classification when using 2 local views for both audio and video.

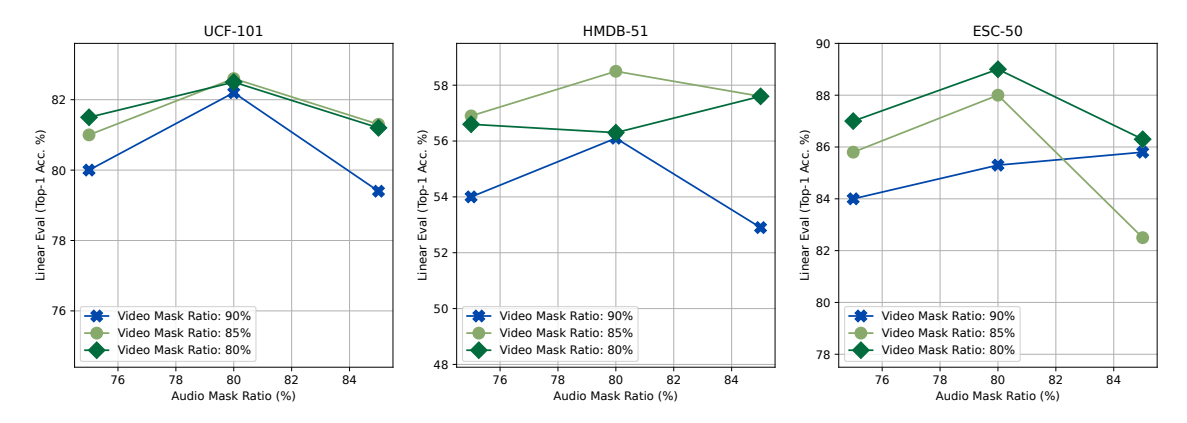


Figure S3. The effect of different masking ratios.

	4096	8192	16384	32768
HMDB51	53.2	58.5	57.0	54.4
UCF101	78.1	82.6	81.5	81.7
ESC50	87.5	88.0	84.1	83.8

Table S6. Effect of different projector output dimensions.

# A.5. Projector Head

Here we further explore different setups for the projector head. First, we present the effect of varying the number of layers and output dimensions in Tables S5 and S6. The results show that a projector head consisting of 3 layers performs most steadily on all the datasets. We also find that an output dimension of 8192 shows stable performance on all the downstream benchmarks.

# A.6. Mask Ratio

We study the effect of different amounts of masking ratios in our proposed framework. Specifically, we test different combinations of audio-masking ratio vs. video-masking ratio to test if there is an internal dependency that might result in optimal performance for both modalities. We sweep a wide ranges of mask ratios, particularly  $\{0.80, 0.85, 0.90\}$ for video masking and  $\{0.75, 0.80, 0.85\}$  for audio masking. The results presented in Figure S3 show that a video mask ratio of 85% and an audio mask ratio of 80% work well on both UCF101 and HMDB51. However, we notice that a slightly lower video mask ratio (e.g., 80%) improves audio performance. We conjecture that this setup benefits from the availability of more visual patches which provides better supervision through cross-modal knowledge distillation. Please note that unless stated otherwise, we use a visual mask ratio of 85% and an audio mask ratio of 80%.

# A.7. Training schedule

In Figure S4, we present the effect of longer pretraining schedules on video action classification for both teacher and

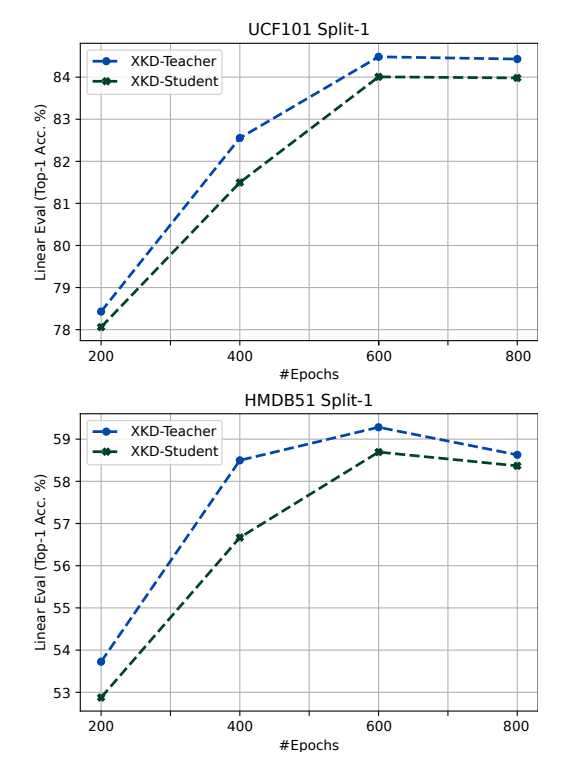


Figure S4. Pretraining epochs vs. downstream evaluation accuracy.

student networks. We pretrain the XKD for up to 800 epochs and find that pretraining for around 600 epochs shows improvement, while beyond that point, a slight performance drop is noticed on HMDB51 and no change is noticed on UCF101. Moreover, we find that the teacher always outperforms the student in downstream evaluation.

#### **B.** Datasets

Here we present the details of the datasets used in this study.

Kinetics400. Kinetics400 [31] is a large-scale action recog-

nition audio-visual dataset consisting of 400 action classes. It has a total of 240K video clips with an average duration of 10 seconds. Following [5, 22, 40, 48, 53], we use the Kinetics400 for both pretraining and downstream evaluation. **UCF101 and HMDB51.** UCF101 [50] and HMDB51 [33] are two of the most popular action recognition datasets used for downstream evaluation. UCF101 consists of a total of 13K clips spread over 101 action classes. HMDB51 contains 7K video clips distributed over 51 action classes. Following [2, 3, 5, 45, 48] both datasets are used for downstream evaluation purposes.

**Kinetics-Sound.** Kinetics-Sound [6] is originally a subset of Kinetics400, which has a total of 22K video clips consisting of 32 action classes. Following [48], we use Kinetics-Sound for multimodal fusion, in addition to uni-modal audio- and video-based action classification. We particularly choose Kinetics-Sound for multimodal evaluation as it consists of hand-picked samples from Kinetics400 which are prominently manifested both audibly and visually.

**ESC50.** ESC50 is a popular sound classification dataset that consists of a total of 2K samples of 50 environmental sound classes, with an average duration of 5 seconds. Following [2, 40, 45, 48], we use ESC50 for downstream evaluation of audio representations.

**FSD50K.** FSD50K is a popular audio dataset of humanlabeled sound events, which consists of 50K audio samples distributed over 200 classes. Moreover, FSD50K is a multi-labeled dataset, where samples are between 0.3 to 30 seconds. Following [41] We use FSD50K for downstream evaluation of audio representations.

# C. Pre-training Details

Here we present the detailed setup of self-supervised pretraining.

# C.1. Augmentation

We adopt standard augmentation strategies [14,41,48] to create the global and local views from the raw audio and visual streams. Particularly, we apply Multi-scale crop, Color Jitter, and Random Horizontal Flip to create global visual views. To create local views, we apply Gray Scale and Gaussian Blur, in addition to the augmentations applied on the global views with minor changes in the augmentation parameters. For example, different from global visual views, we apply aggressive cropping to create local visual views. The details of the augmentation parameters are presented in Table S7. Next, simple Volume Jitter is applied on the audio stream to create the global audio views. We apply Random Crop in addition to the Volume Jitter to create the local audio views. The details of the audio augmentation parameters are presented in Table S8.

Augmentation	Param	Global View	Local View	Linear Eval.
Multi-Scale Crop	Crop Scale	[0.2, 1]	[0.08, 0.4]	[0.08, 1]
Horizontal Flip	Probability	0.5	0.5	0.5
	Brightness	0.4	0.4	0.4
Color litter	Contrast	0.4	0.4	0.4
Color Jiller	Saturation	0.4	0.4	0.4
	Hue	0.2	0.2	0.2
Gray Scale	Probability	n/a	0.2	0.2
Gaussian Blur	Probability	n/a	0.5	n/a

Table S7. Visual augmentation parameters. n/a: not applied.

Augmentation	Param	Global View	Local View	Linear Eval.
Volume Jitter	Scale	± 0.1	± 0.2	± 0.1
Random Crop	Range Crop Scale	n/a n/a	[0.6, 1.5] [1, 1.5]	n/a n/a

Table S8. Audio augmentation parameters. n/a: not applied.

Variant	Input Projection	Teacher	Student	Decoder
XKD-MAS	NS	NS	S	NS
XKD-MATS	NS	S	S	NS
XKD-MAT	NS	S	NS	NS
XKD	NS	NS	NS	NS

Table S9. Summary of parameter sharing in modality-agnostic setups. Here, *S* and *NS* refer to shared and not-shared parameters between audio and visual modalities respectively.

# C.2. Modality-agnostic Network

In Table S9, we summarize the detailed network setups of the modality-agnostic variants.

# C.3. Implementation Details

We train XKD using an AdamW [34,46] optimizer and warm-up cosine learning rate scheduler for 800 epochs. Please note that for the ablation studies, the models are trained for 400 epochs. We use ViT-B [21] as the backbone/encoder for both audio and visual modalities. Following [29], we use a shallow decoder for reconstruction and adopt a similar projector head to the one proposed in [13]. Please see the additional architecture details in Table \$10. We perform distributed training with a batch size of 256 using 8 NVIDIA V100 32 GB GPUs in parallel. As mentioned in Table \$10, we use visual frames with resolutions of 96<sup>2</sup> and  $112^2$ , which allows us to train the proposed XKD with a limited computation setup. Additionally, we perform mixedprecision [36] training to save the computation overhead. In our setup, it takes approximately 5 days to train the XKD for 400 epochs. We present the additional details for the training parameters in Table \$11.

Name	Value
Video Input Resolution (global) Video Input Resolution (local) Video Patch Size	$32 \times 112^{2}$ $8 \times 96^{2}$ $4 \times 16^{2}$
Audio Input Resolution (global) Audio Input Resolution (local) Audio Patch Size	$80 \times 448$ $80 \times 112$ $4 \times 16$
Backbone/Encoder	ViT-Base (87M) embed dim:768 depth:12 num heads:12
Decoder	Transformer embed dim:384 depth:4 num heads:12
Projector	MLP out dim: 8192 bottleneck dim: 256 hidden dim: 2048 num layers: 3

Table S10. Network-related parameters in pretraining.

Name	Value
Epochs	800
Batch Size	256
Optimizer	AdamW
Optimizer Betas	[0.9, 0.95]
LR Scheduler	Cosine
LR Warm-up Epochs	30
LR Warm-up	0
LR Base	0.0001
LR Final	0
Weight Decay	0.3
EMA Scheduler	Cosine
EMA Base	0.997
EMA Final	1
Video Mask Ratio	0.85%
Audio Mask Ratio	0.80%
Video Student Temp.	0.1
Audio Student Temp.	0.1
Video Teacher Temp.	0.1
Audio Teacher Temp.	0.07
Center Momentum	0.9

Table S11. Kinetics400 pretraining parameters.

# **D. Downstream Evaluation Protocol**

We perform downstream evaluations on 6 different datasets in 8 different setups. The details of the evaluation setups are as follows.

# **D.1. Linear Evaluation**

#### **D.1.1 UCF101 and HMDB51**

To perform linear evaluation, we feed 32 frames with a spatial resolution of  $112^2$  to the pretrained visual encoder. We extract the fixed features as the mean of all the patches from the last layer of the encoder. We randomly select 25 samples per clip during training, while during testing, we uniformly fetch 3 clips per sample to extract frozen features. Next, the features are used for action classification using a linear SVM kernel. We sweep a range of cost values  $\{0.00001, 0.0001, 0.001, 0.01, 0.1, 1\}$  and report the best top-1 accuracy. We present the augmentation parameters applied on the training set in Table S7. Please note that none of the augmentations are applied to the test set. We then tune the models using split 1 of the datasets and report the top-1 accuracies averaged over all the splits.

#### D.1.2 ESC50

We feed 4 seconds of audio input to the pretrained audio encoder and extract approximately 10-epochs worth of fixed features. Similar to UCF101 and HMDB51 we extract the features as the mean of all the patches from the last layer of the encoder. During training, we apply Volume Jitter as augmentation and no augmentation is applied at test time. Similar to the setup of UCF101 and HMDB51, we sweep the same range of cost values to find the best model. We report the final top-1 accuracy averaged over all the splits.

# D.1.3 FSD50K

To perform the downstream evaluation on FSD50K we follow the same setup as ESC50, with the exception of using a linear fully-connected layer instead of SVM. During training, we randomly extract 10 clips per sample and feed them to the pretrained audio encoder. Moreover, during test, we uniformly select 8 clips per sample and report the mean average precision (mAP) [24]. The extracted features are used to train a fully-connected layer using an AdamW [34, 46] optimizer for 50 epochs at a fixed learning rate of 0.001. Moreover, we apply weight decay of 1e-5 and dropout of 0.3 to prevent overfitting. We use a batch size of 256 and train on a single RTX6000 24 GB NIVIDIA GPU.

# D.1.4 Kinetics-Sound and Kinetics400

We use Kinetics-Sound for uni-modal evaluations using audio and visual representations separately, as well as multi-modal evaluation using late fusion. For uni-modal evaluation, we follow similar setups to UCF101 and ESC50 for visual and audio representations, respectively. During, multimodal fusion, we simply concatenate the corresponding audio and visual features, and the joint representations are then directly

Name	Value
Epochs	100
Batch Size	96
Optimizer	AdamW
Optimizer Betas	[0.9, 0.999]
LR Scheduler	Cosine
LR Warm-up Epochs	30
LR Warm-up	0
LR Base	0.0005
LR Final	$1.0e^{-06}$
Weight Decay	0.05
RandAug	(9, .05)
Label Smoothing	0.1
MixUp	0.6
CutMix	0.5
Drop Path	0
Dropout	0.5
Layer-wise LR Decay	0.45

Table S12. Kinetics400 fine-tuning parameters.

used to perform action classification using a linear kernel SVM. Finally, we report the top-1 accuracy in all the setups.

We follow similar setups to those used for UCF101 and HMDB51 to perform linear evaluation on Kinetics400, with the exception of randomly sampling 3 clips per video during training and testing to extract the features (we do not sample more clips during training due to memory constraints). Lastly, we report top-1 and top-5 accuracies in action classification.

# **D.2. Fine-tuning**

#### **D.2.1** Kinetics400

We use the pretrained visual encoder and add a fullyconnected layer to finetune on Kinetics400. Different from our pretraining setup, we use a spatial resolution of  $224^2$ in finetuning. During training, we apply Random Augmentation [18] in addition to Multi-scale Crop and Random Horizontal Flip on the visual data, similar to [22, 29, 53]. We use an AdamW [34, 46] optimizer to train the network for 100 epochs using a cosine learning rate scheduler. In addition to the cosine learning rate scheduler, we employ layer-wise-layer-decay [12] which further stabilizes the training. We perform distributed training with a batch size of 96 using 16 NVIDIA V100 32 GB GPUs in parallel. Additionally, we employ MixUp [56], CutMix [55], and label smoothing [51], which boosts the fine-tuning performance. We present the details of the finetuning parameters in Table S12. During training, we randomly sample 1 clip per sample, while during testing, 3 clips are uniformly selected per sample. We report the sample level prediction (top-1 and top-5 accuracy) averaged over all the clips. Please note that we obtain the results for VideoMAE<sup>1</sup> [53] in Table 5 using their officially released code. Different from their original

implementation, we pretrain their model using a batch size of 256 and finetune with a batch size of 96, identical to our setup (also due to limited computation resources).

# References

- [1] Triantafyllos Afouras, Joon Son Chung, and Andrew Zisserman. Asr is all you need: Cross-modal distillation for lip reading. In *ICASSP*, pages 2143–2147. IEEE, 2020. 1, 2
- [2] Hassan Akbari, Liangzhe Yuan, Rui Qian, Wei-Hong Chuang, Shih-Fu Chang, Yin Cui, and Boqing Gong. Vatt: Transformers for multimodal self-supervised learning from raw video, audio and text. *NeurIPS*, 34, 2021. 1, 2, 3, 5, 7, 8, 12
- [3] Jean-Baptiste Alayrac, Adria Recasens, Rosalia Schneider, Relja Arandjelovic, Jason Ramapuram, Jeffrey De Fauw, Lucas Smaira, Sander Dieleman, and Andrew Zisserman. Self-supervised multimodal versatile networks. *NeurIPS*, 2(6):7, 2020. 2, 7, 12
- [4] Samuel Albanie, Arsha Nagrani, Andrea Vedaldi, and Andrew Zisserman. Emotion recognition in speech using cross-modal transfer in the wild. In *ACM Multimedia*, pages 292–301, 2018. 1, 2
- [5] Humam Alwassel, Dhruv Mahajan, Bruno Korbar, Lorenzo Torresani, Bernard Ghanem, and Du Tran. Self-supervised learning by cross-modal audio-video clustering. *NeurIPS*, 33, 2020. 1, 2, 7, 8, 12
- [6] Relja Arandjelovic and Andrew Zisserman. Look, listen and learn. In *ICCV*, pages 609–617, 2017. 1, 5, 12
- [7] Anurag Arnab, Mostafa Dehghani, Georg Heigold, Chen Sun, Mario Lučić, and Cordelia Schmid. Vivit: A video vision transformer. In *ICCV*, pages 6836–6846, 2021. 5
- [8] Yuki M. Asano, Mandela Patrick, Christian Rupprecht, and Andrea Vedaldi. Labelling unlabelled videos from scratch with multi-modal self-supervision. In *NeurIPS*, 2020. 2
- [9] Yusuf Aytar, Carl Vondrick, and Antonio Torralba. Soundnet: Learning sound representations from unlabeled video. *NeurIPS*, 29, 2016. 1, 2
- [10] Roman Bachmann, David Mizrahi, Andrei Atanov, and Amir Zamir. Multimae: Multi-modal multi-task masked autoencoders. *arXiv preprint arXiv:2204.01678*, 2022. 2
- [11] Alexei Baevski, Wei-Ning Hsu, Qiantong Xu, Arun Babu, Jiatao Gu, and Michael Auli. Data2vec: A general framework for self-supervised learning in speech, vision and language. *arXiv preprint arXiv:2202.03555*, 2022. 3, 4
- [12] Hangbo Bao, Li Dong, and Furu Wei. Beit: Bert pre-training of image transformers. *arXiv preprint arXiv:2106.08254*, 2021. 2, 3, 14

- [13] Mathilde Caron, Hugo Touvron, Ishan Misra, Hervé Jégou, Julien Mairal, Piotr Bojanowski, and Armand Joulin. Emerging properties in self-supervised vision transformers. In *ICCV*, pages 9650–9660, 2021. 4, 5, 9, 12
- [14] Ting Chen, Simon Kornblith, Mohammad Norouzi, and Geoffrey Hinton. A simple framework for contrastive learning of visual representations. In *ICML*, pages 1597–1607, 2020. 1, 12
- [15] Xinlei Chen and Kaiming He. Exploring simple siamese representation learning. In *CVPR*, pages 15750–15758, 2021. 1
- [16] Yanbei Chen, Yongqin Xian, A Koepke, Ying Shan, and Zeynep Akata. Distilling audio-visual knowledge by compositional contrastive learning. In *CVPR*, pages 7016–7025, 2021. 1, 2, 6
- [17] Dading Chong, Helin Wang, Peilin Zhou, and Qingcheng Zeng. Masked spectrogram prediction for self-supervised audio pre-training. *arXiv* preprint *arXiv*:2204.12768, 2022. 2, 7
- [18] Ekin D Cubuk, Barret Zoph, Jonathon Shlens, and Quoc V Le. Randaugment: Practical automated data augmentation with a reduced search space. In *CVPRW*, pages 702–703, 2020. 14
- [19] Rui Dai, Srijan Das, and François Bremond. Learning an augmented rgb representation with cross-modal knowledge distillation for action detection. In *ICCV*, pages 13053–13064, 2021. 2
- [20] Jacob Devlin, Ming-Wei Chang, Kenton Lee, and Kristina Toutanova. Bert: Pre-training of deep bidirectional transformers for language understanding. arXiv preprint arXiv:1810.04805, 2018. 1, 2, 3
- [21] Alexey Dosovitskiy, Lucas Beyer, Alexander Kolesnikov, Dirk Weissenborn, Xiaohua Zhai, Thomas Unterthiner, Mostafa Dehghani, Matthias Minderer, Georg Heigold, Sylvain Gelly, et al. An image is worth 16x16 words: Transformers for image recognition at scale. arXiv preprint arXiv:2010.11929, 2020. 1, 5, 12
- [22] Christoph Feichtenhofer, Haoqi Fan, Yanghao Li, and Kaiming He. Masked autoencoders as spatiotemporal learners. *arXiv preprint arXiv:2205.09113*, 2022. 1, 2, 5, 7, 12, 14
- [23] Christoph Feichtenhofer, Haoqi Fan, Bo Xiong, Ross Girshick, and Kaiming He. A large-scale study on unsupervised spatiotemporal representation learning. In CVPR, pages 3299–3309, 2021.
- [24] Eduardo Fonseca, Xavier Favory, Jordi Pons, Frederic Font, and Xavier Serra. FSD50K: an open dataset of human-labeled sound events. *IEEE/ACM Transactions* on Audio, Speech, and Language Processing, 30:829– 852, 2022. 1, 5, 8, 13

- [25] Rohit Girdhar, Mannat Singh, Nikhila Ravi, Laurens van der Maaten, Armand Joulin, and Ishan Misra. Omnivore: A single model for many visual modalities. In *CVPR*, pages 16102–16112, 2022. 1, 2
- [26] Yuan Gong, Yu-An Chung, and James Glass. Ast: Audio spectrogram transformer. *arXiv preprint arXiv:2104.01778*, 2021. 1, 2, 3, 5, 7
- [27] Arthur Gretton, Karsten Borgwardt, Malte Rasch, Bernhard Schölkopf, and Alex Smola. A kernel method for the two-sample-problem. *NeurIPS*, 19, 2006. 4
- [28] Jean-Bastien Grill, Florian Strub, Florent Altché, Corentin Tallec, Pierre Richemond, Elena Buchatskaya, Carl Doersch, Bernardo Pires, Zhaohan Guo, Mohammad Azar, et al. Bootstrap your own latent: A new approach to self-supervised learning. In *NeurIPS*, 2020.
- [29] Kaiming He, Xinlei Chen, Saining Xie, Yanghao Li, Piotr Dollár, and Ross Girshick. Masked autoencoders are scalable vision learners. arXiv preprint arXiv:2111.06377, 2021. 1, 2, 3, 5, 12, 14
- [30] Longlong Jing, Xiaodong Yang, Jingen Liu, and Yingli Tian. Self-supervised spatiotemporal feature learning via video rotation prediction. *arXiv preprint arXiv:1811.11387*, 2018. 2
- [31] Will Kay, Joao Carreira, Karen Simonyan, Brian Zhang, Chloe Hillier, Sudheendra Vijayanarasimhan, Fabio Viola, Tim Green, Trevor Back, Paul Natsev, et al. The kinetics human action video dataset. *arXiv preprint arXiv:1705.06950*, 2017. 1, 5, 11
- [32] Khaled Koutini, Jan Schlüter, Hamid Eghbal-zadeh, and Gerhard Widmer. Efficient training of audio transformers with patchout. *arXiv preprint arXiv:2110.05069*, 2021. 7
- [33] Hildegard Kuehne, Hueihan Jhuang, Estíbaliz Garrote, Tomaso Poggio, and Thomas Serre. Hmdb: a large video database for human motion recognition. In *ICCV*, pages 2556–2563, 2011. 1, 5, 12
- [34] Ilya Loshchilov and Frank Hutter. Decoupled weight decay regularization. *arXiv preprint arXiv:1711.05101*, 2017. 12, 13, 14
- [35] Shuang Ma, Zhaoyang Zeng, Daniel McDuff, and Yale Song. Active contrastive learning of audio-visual video representations. In *ICLR*, 2020. 1
- [36] Paulius Micikevicius, Sharan Narang, Jonah Alben, Gregory Diamos, Erich Elsen, David Garcia, Boris Ginsburg, Michael Houston, Oleksii Kuchaiev, Ganesh Venkatesh, et al. Mixed precision training. In *ICLR*, 2018. 12
- [37] Shaobo Min, Qi Dai, Hongtao Xie, Chuang Gan, Yongdong Zhang, and Jingdong Wang. Cross-modal atten-

- tion consistency for video-audio unsupervised learning. *arXiv preprint arXiv:2106.06939*, 2021. 1
- [38] Ishan Misra and Laurens van der Maaten. Selfsupervised learning of pretext-invariant representations. In *CVPR*, pages 6707–6717, 2020. 1
- [39] Pedro Morgado, Ishan Misra, and Nuno Vasconcelos. Robust audio-visual instance discrimination. In *CVPR*, pages 12934–12945, 2021. 1, 2
- [40] Pedro Morgado, Nuno Vasconcelos, and Ishan Misra. Audio-visual instance discrimination with cross-modal agreement. In *CVPR*, pages 12475–12486, 2021. 1, 2, 7, 8, 12
- [41] Daisuke Niizumi, Daiki Takeuchi, Yasunori Ohishi, Noboru Harada, and Kunio Kashino. Byol for audio: Exploring pre-trained general-purpose audio representations. *arXiv preprint arXiv:2204.07402*, 2022. 7, 8, 12
- [42] Daisuke Niizumi, Daiki Takeuchi, Yasunori Ohishi, Noboru Harada, and Kunio Kashino. Masked spectrogram modeling using masked autoencoders for learning general-purpose audio representation. *arXiv preprint arXiv:2204.12260*, 2022. 2, 3
- [43] Karol J. Piczak. ESC: Dataset for Environmental Sound Classification. In *ACM Multimedia*, pages 1015–1018. , 2015. 1, 5, 8
- [44] Rui Qian, Tianjian Meng, Boqing Gong, Ming-Hsuan Yang, Huisheng Wang, Serge Belongie, and Yin Cui. Spatiotemporal contrastive video representation learning. In *CVPR*, pages 6964–6974, 2021. 2
- [45] Adrià Recasens, Pauline Luc, Jean-Baptiste Alayrac, Luyu Wang, Florian Strub, Corentin Tallec, Mateusz Malinowski, Viorica Patraucean, Florent Altché, Michal Valko, et al. Broaden your views for self-supervised video learning. arXiv preprint arXiv:2103.16559, 2021. 2, 7, 12
- [46] Sashank J Reddi, Satyen Kale, and Sanjiv Kumar. On the convergence of adam and beyond. *arXiv preprint arXiv:1904.09237*, 2019. 12, 13, 14
- [47] Sucheng Ren, Yong Du, Jianming Lv, Guoqiang Han, and Shengfeng He. Learning from the master: Distilling cross-modal advanced knowledge for lip reading. In *CVPR*, pages 13325–13333, 2021. 1, 2, 6
- [48] Pritam Sarkar and Ali Etemad. Self-supervised audiovisual representation learning with relaxed cross-modal temporal synchronicity, 2021. 1, 2, 7, 8, 12
- [49] Madeline C Schiappa, Yogesh S Rawat, and Mubarak Shah. Self-supervised learning for videos: A survey. *arXiv preprint arXiv:2207.00419*, 2022. 2
- [50] Khurram Soomro, Amir Roshan Zamir, and Mubarak Shah. Ucf101: A dataset of 101 human actions

- classes from videos in the wild. arXiv preprint arXiv:1212.0402, 2012. 1, 5, 12
- [51] Christian Szegedy, Vincent Vanhoucke, Sergey Ioffe, Jon Shlens, and Zbigniew Wojna. Rethinking the inception architecture for computer vision. In CVPR, pages 2818–2826, 2016. 14
- [52] Antti Tarvainen and Harri Valpola. Mean teachers are better role models: Weight-averaged consistency targets improve semi-supervised deep learning results. *NeurIPS*, 30, 2017. 3, 4, 8
- [53] Zhan Tong, Yibing Song, Jue Wang, and Limin Wang. Videomae: Masked autoencoders are data-efficient learners for self-supervised video pre-training. *arXiv* preprint arXiv:2203.12602, 2022. 2, 3, 5, 7, 8, 12, 14
- [54] Rui Wang, Dongdong Chen, Zuxuan Wu, Yinpeng Chen, Xiyang Dai, Mengchen Liu, Yu-Gang Jiang, Luowei Zhou, and Lu Yuan. Bevt: Bert pretraining of video transformers. *arXiv preprint arXiv:2112.01529*, 2021. 2, 3, 7, 8
- [55] Sangdoo Yun, Dongyoon Han, Seong Joon Oh, Sanghyuk Chun, Junsuk Choe, and Youngjoon Yoo. Cutmix: Regularization strategy to train strong classifiers with localizable features. In *ICCV*, pages 6023– 6032, 2019. 14
- [56] Hongyi Zhang, Moustapha Cisse, Yann N Dauphin, and David Lopez-Paz. mixup: Beyond empirical risk minimization. *arXiv preprint arXiv:1710.09412*, 2017. 14